

Albedos of Main-Belt Comets 133P/Elst-Pizarro and 176P/LINEAR ¹Henry H. Hsieh^a, David Jewitt^b, and Yanga R. Fernández^c^a*Astrophysics Research Centre, Queen's University, Belfast, BT7 1NN, United Kingdom*^b*Institute for Astronomy, University of Hawaii, 2680 Woodlawn Drive, Honolulu, HI 96822, USA*^c*Univ. of Central Florida, M.A.P. Building, 4000 Central Florida Blvd., Orlando, FL 32816, USA*

h.hsieh@qub.ac.uk, jewitt@ifa.hawaii.edu, yfernandez@physics.ucf.edu

ABSTRACT

We present the determination of the geometric R -band albedos of two main-belt comet nuclei based on data from the Spitzer Space Telescope and a number of ground-based optical facilities. For 133P/Elst-Pizarro, we find an albedo of $p_R = 0.05 \pm 0.02$ and an effective radius of $r_e = 1.9 \pm 0.3$ km (estimated semi-axes of $a \sim 2.3$ km and $b \sim 1.6$ km). For 176P/LINEAR, we find an albedo of $p_R = 0.06 \pm 0.02$ and an effective radius of $r_e = 2.0 \pm 0.2$ km (estimated semi-axes of $a \sim 2.6$ km and $b \sim 1.5$ km). In terms of albedo, 133P and 176P are similar to each other and are typical of other Themis family asteroids, C-class asteroids, and other comet nuclei. We find no indication that 133P and 176P are compositionally unique among other dynamically-similar (but inactive) members of the Themis family, in agreement with previous assertions that the two objects most likely formed in-situ. We also note that low albedo ($p_R < 0.075$) remains a consistent feature of all cometary (*i.e.*, icy) bodies, whether they originate in the inner solar system (the main-belt comets) or in the outer solar system (all other comets).

Subject headings: comets: general — minor planets, asteroids

¹This work makes use of observations made with the Spitzer Space Telescope (Programs 3119 and 30678), which is operated by the Jet Propulsion Laboratory, California Institute of Technology under a contract with the National Aeronautics and Space Administration (NASA). Additionally, some data presented herein were obtained at the W. M. Keck Observatory, which is operated as a scientific partnership among the California Institute of Technology, the University of California, and NASA, and was made possible by the generous financial support of the W. M. Keck Foundation. Some data presented herein were also obtained at ESO facilities at La Silla under program ID 081.C-0822(A).

1. INTRODUCTION

The main-belt comets (MBCs), of which 133P/Elst-Pizarro (hereafter, 133P) and 176P/LINEAR (hereafter, 176P) are examples, occupy stable orbits that are decoupled from Jupiter and which are indistinguishable from the orbits of other main-belt asteroids (Hsieh & Jewitt 2006b). Dynamical simulations show that MBCs are extremely unlikely to originate in the Kuiper Belt given the current configuration of the major planets (*e.g.*, Fernández *et al.* 2002), indicating that they are instead likely to be native to the main asteroid belt. Recent work suggests that some icy Kuiper Belt objects might have been delivered to the asteroid belt during the Late Heavy Bombardment (Levison *et al.* 2008), but even those simulations fail to produce the low-inclination, low-eccentricity orbits of MBCs such as 133P and 176P.

In this letter, we use observations from the Spitzer Space Telescope (hereafter, Spitzer; Werner *et al.* 2004) to determine the geometric albedos of 133P and 176P, and then discuss the implications of these measurements.

2. OBSERVATIONS

We obtained optical observations of 133P and 176P on multiple occasions from 2003 through 2008 using the 10 m Keck I and University of Hawaii (UH) 2.2 m telescopes on Mauna Kea, and the 3.58 m New Technology Telescope (NTT) at the European Southern Observatory (ESO) at La Silla. Observations with the UH 2.2 m telescope were made using either a Tektronix 2048×2048 pixel CCD or the Orthogonal Parallel Transfer Imaging Camera (OPTIC; Tonry *et al.* 2004), both behind standard Kron-Cousins BVRI broadband filters. Observations with Keck were made using the Low Resolution Imaging Spectrometer (LRIS; Oke *et al.* 1995) in imaging mode. LRIS employs a Tektronix 2048 × 2048 CCD with standard Kron-Cousins BVRI filters. Observations with the NTT were made using the ESO Faint Object Spectrograph and Camera (EFOSC2; Buzzoni *et al.* 1984), which employs a 2048×2048 pixel Loral/Lesser CCD behind Bessel BVR broadband filters.

Bias subtraction and flat-field reduction were performed for all optical data. Dithered images of the twilight sky were used to construct flat fields for UH 2.2 m data, while images of the illuminated interior of the telescope dome were used to construct flat fields for Keck and NTT data. Photometry of our target objects and Landolt (1992) standard stars was obtained by measuring net fluxes within circular apertures of varying radii depending on the nightly seeing, with background sampled from surrounding circular annuli.

Spitzer observations of 133P (3 visits, 166 s of total exposure time per visit; Fig. 1a), using the 24 μm channel (effective wavelength of 23.68 μm) of the Multiband Imaging Photometer for Spitzer (MIPS; Rieke *et al.* 2004) and originally obtained on 2005 April 11 as part of Cycle 1 program 3119 (Reach *et al.* 2007), were retrieved from the Spitzer archive. Observations of 176P (2 visits, 48 s of total exposure time per visit; Fig. 1b), also with the 24 μm channel of MIPS, were obtained

on 2007 January 1 as part of Cycle 3 program 30678. Observational circumstances are shown in Table 1. Photometry of our target objects from pipeline-processed Spitzer post-Basic Calibrated Data (PBCD) was obtained by measuring net fluxes within circular apertures with 6-pixel ($14''.7$) radii, and then applying appropriate aperture corrections (1.14 in the case of a 6-pixel aperture) and color corrections (0.96 for both targets).

3. RESULTS

We use our optical data to find best-fit IAU phase function parameters for 133P of $H_R = 15.49 \pm 0.05$ mag and $G = 0.04 \pm 0.05$, and best-fit linear phase function parameters (omitting data obtained at solar phase angles at which opposition surge effects are expected) of $m_R(1, 1, 0) = 15.69 \pm 0.05$ mag and $\beta = 0.049 \pm 0.004$ mag deg $^{-1}$. These parameters are calculated using photometry obtained while 133P was observed to be inactive, and as such, are a refinement of parameters previously derived by Hsieh *et al.* (2004) from photometry obtained while 133P was visibly active. For 176P, we find corresponding parameters of $H_R = 15.10 \pm 0.05$ mag, $G = 0.26 \pm 0.05$, $m_R(1, 1, 0) = 15.27 \pm 0.05$ mag, and $\beta = 0.034 \pm 0.005$ mag deg $^{-1}$. These parameters were likewise calculated only using photometry obtained while the comet was observed to be inactive. Plots of phase function solutions for both objects are shown in Figure 2. From their phase functions, we estimate our targets' expected mean optical magnitudes as viewed from Spitzer at the time of their observations to be $m_R = 21.63$ mag for 133P and $m_R = 20.39$ mag for 176P.

Both objects exhibit significant rotational brightness variations, however, which represent significant sources of uncertainty in the interpretation of our infrared data. A rotation period of $P_{rot} = 3.471$ hr and a lightcurve range of $\Delta m = 0.4$ mag have been previously found for 133P (Hsieh *et al.* 2004). The rotational properties of 176P are currently poorly constrained. On 2007 March 21, however, we observed a photometric range for the object of $\Delta m \approx 0.6$ mag over ~ 4.5 hr, suggesting a rotation period of $P_{rot} \geq 18$ hr (assuming a double-peaked lightcurve). This is consistent with Licandro *et al.* (2007a) who found $P_{rot} > 22$ hr.

Fortunately, constraints on the rotational phase of each object can be derived from the infrared data. Our second flux density measurement for 176P was 1.4 times larger than the first, implying an equivalent increase in visible cross-sectional area, corresponding to a change in visual magnitude of $\Delta m = -0.37$ mag, a significant fraction of the object's inferred optical photometric range. Such a large magnitude change indicates that the object was necessarily first observed near the minimum and then near the maximum of its lightcurve (consistent with the 4.55 hr interval between the two observations). Using these constraints, we are able to adjust our optical brightness estimates (Table 1) accordingly, thereby reducing the effects of rotational phase uncertainty. The three Spitzer observations of 133P span only 7 min meaning that the rotational phase is less tightly constrained. Given 133P's short rotation period, however, a small decrease in the scattering cross-section is still detectable between the first and last Spitzer observation, corresponding to a change in visual magnitude of $\Delta m = 0.14$ mag and leading to the revised optical brightness estimates for 133P in

Table 1.

We use the Harris (1998) Near-Earth Asteroid Thermal Model (NEATM) to iteratively solve for the effective radius, r_e , and geometric R -band albedo, p_R , of each object. As with any model, NEATM requires a number of assumptions, which, in turn, introduce uncertainties. One such source of uncertainty is the phase effect for thermal emission. NEATM treats the effect geometrically, calculating it based on the fraction of the Earth-facing hemisphere that is illuminated by the Sun at the time of observation. While this effect has been poorly measured and thus poorly constrained for large phase angles, the infrared phase coefficient of $0.01 \text{ mag deg}^{-1}$ that we use here is generally considered to be appropriate for phase angles $\alpha < 30^\circ$ (*cf.* Morrison 1977; Harris 1998). Thus, given the small phase angles ($14^\circ < \alpha < 17^\circ$) at which the Spitzer observations were obtained, this effect should introduce minimal systematic uncertainty into our calculations.

A more significant issue is that of the beaming parameter, η . We lack the minimum number of data points needed to constrain η for either 133P or 176P, forcing us to assume its value. A Spitzer survey of ~ 50 Jupiter-family comet nuclei by Fernández *et al.* (2008), however, found values of $0.6 < \eta < 1.2$, and all were consistent with $\eta \approx 0.94 \pm 0.20$. Given the results of this survey and assuming that 133P and 176P have low thermal inertias (similar to other comet nuclei, *e.g.*, 9P/Tempel 1, which has $I < 50 \text{ W K}^{-1} \text{ m}^{-2} \text{ s}^{1/2}$; Groussin *et al.* 2007), we adopt $\eta = 1.0$ as a reasonable assumption for solving for r_e and p_R . To account for uncertainties in η , we also perform parallel calculations for $\eta = 0.8$ and $\eta = 1.2$ (Table 2).

Thus, assuming an emissivity of $\varepsilon = 0.9$, we find $r_e = 1.9 \pm 0.3 \text{ km}$ and $p_R = 0.05 \pm 0.02$ for 133P, and $r_e = 2.0 \pm 0.2 \text{ km}$ and $p_R = 0.06 \pm 0.02$ for 176P. Estimated errors for both objects are mainly due to uncertainties in both η and rotational phase. Given the observed photometric ranges ($\Delta m_{133P} \approx 0.40 \text{ mag}$; $\Delta m_{176P} \approx 0.60 \text{ mag}$) and corresponding inferred minimum axis ratios ($[a/b]_{133P} \approx 1.45$; $[a/b]_{176P} \approx 1.74$) for each object, we find $a \sim 2.3 \text{ km}$ and $b \sim 1.6 \text{ km}$ for 133P, and $a \sim 2.6 \text{ km}$ and $b \sim 1.5 \text{ km}$ for 176P as our best estimates of the semiaxes of each object.

4. DISCUSSION

We plot histograms showing the albedo (p_V) distributions of several solar system body populations of interest in Figure 3. Assuming that both 133P and 176P are approximately spectrally neutral (*i.e.*, $p_V \approx p_R$), based on 133P’s spectral classification as a C- or B-type asteroid and 176P’s classification as a B-type asteroid (Licandro *et al.* 2007a), we find that their albedos are typical of C-class asteroids (Fig. 3a) and are also well within the distribution of albedos measured for members of the Themis asteroid family (Fig. 3b), with which 133P and 176P appear to be dynamically associated (Hsieh & Jewitt 2006b).

The Themis family is dominated by C-class asteroids (*cf.* Florczak *et al.* 1999), of which a substantial fraction (17 of the 39 currently classified members of the family, or $\sim 44\%$) belong to the subclass of B-type asteroids. For comparison, B-type asteroids comprise only $\sim 15\%$ of the

general C-class population and $\sim 5\%$ of all currently classified asteroids (Tholen & Barucci 1989; Lazzaro *et al.* 2004). In terms of albedo, we find 133P and 176P to be consistent with both C-type asteroids and B-type asteroids (*cf.* Figs. 3a and 3d), in agreement with their spectral classifications by Licandro *et al.* (2007a). Thus, in terms of both albedo and spectral type, 133P and 176P appear to be typical Themis asteroids, supporting previous speculation that the family might be home to more MBCs (Hsieh & Jewitt 2006a).

Other objects like 133P and 176P that also have orbits considered to be dynamically asteroidal, yet have been associated with observed or inferred cometary activity, are also classified as C-class objects. One such object is the cross-listed comet-asteroid 107P/(4015) Wilson-Harrington (C- or F-type; Tholen & Barucci 1989). Other examples include Geminid meteor stream parent 3200 Phaethon (B- or F-type; Tholen & Barucci 1989; Licandro *et al.* 2007b) and its possible fragment, 155140 (2005 UD) (B- or F-type; Jewitt & Hsieh 2006; Kinoshita *et al.* 2007). Another likely fragment of 3200 Phaethon, 1999 YC, appears spectrally neutral and is classified as a C-type object (Kasuga & Jewitt 2008).

Being below the upper bound of “comet-like” albedos ($p_R = 0.075$) employed by Fernández *et al.* (2005), the albedos of 133P and 176P are also consistent with those of the nuclei of other active comets (Fig. 3d). Spectroscopically, comet nuclei exhibit a broad range of colors, with both D-type-like and C-type-like spectral reflectivity gradients being found for various comets (*cf.* Fitzsimmons *et al.* 1994; Jewitt 2002), and in terms of albedos, the two MBC nuclei we consider here are consistent with both spectral types (Fig. 3a & 3e). Thus, despite their strong dynamical association with main-belt asteroids, we find that 133P and 176P have surfaces that may be compositionally comparable to other comets. This is consistent with Jewitt (2002) who suggested that the surface properties of short-period comet nuclei were likely largely due to sublimation-driven evolutionary effects and were not primordial in nature.

Studying the surface properties of the main-belt comets is vital for understanding their evolution and putting their volatile content into the proper context. In light of those goals, we find that, in terms of albedos, (1) 133P and 176P are similar to each other, (2) they are typical of other Themis asteroids and the C- and B-type asteroids that dominate the Themis family, and (3) their albedos are also consistent with albedos measured for other comet nuclei and D-type asteroids. Given these results, we find that low albedo continues to be a consistent feature of all cometary bodies, whether they originate in the outer or inner solar system. This finding necessarily also means, however, that albedo does not appear to be an effective diagnostic of the region from which a comet originates.

We acknowledge support of this work through STFC fellowship grant ST/F011016/1 to HHH, NASA Spitzer grant JPL-1289078 and NASA Planetary Astronomy grant NNG05GF76G to DJ, and NASA grant JPL-1289123 to YRF. We also thank Bill Reach for valuable discussion and Alan Harris (DLR, Berlin) for pointing out an error in our initial albedo calculations.

REFERENCES

- Brownlee, D. E., Horz, F., Newburn, R. L., Zolensky, M., Duxbury, T. C., Sandford, S., Sekanina, Z., Tsou, P., Hanner, M. S., Clark, B. C., Green, S. F., & Kissel, J. 2004, *Science*, 304, 1764
- Buzzoni, B., Delabre, B., Dekker, H., Dodorico, S., Enard, D., Focardi, P., Gustafsson, B., Nees, W., Paureau, J., & Reiss, R. 1984, *The Messenger*, 38, 9
- Fernández, J. A., Gallardo, T., & Brunini, A. 2002, *Icarus*, 159, 358
- Fernández, Y. R., Jewitt, D. C., & Sheppard, S. S. 2005, *AJ*, 130, 308
- Fernández, Y. R., Kelley, M. S., Lamy, P. L., Toth, I., Groussin, O., A'Hearn, M. F., Bauer, J. M., Campins, H., Fitzsimmons, A., Licandro, J., Lisse, C. M., Lowry, S. C., Meech, K. J., Pittichová, J., Reach, W. T., Snodgrass, C., & Weaver, H. A. 2008, *LPI Contributions*, 1405, 8307
- Fitzsimmons, A., Dahlgren, M., Lagerkvist, C.-I., Magnusson, P., & Williams, I. P. 1994, *A&A*, 282, 634
- Florczak, M., Lazzaro, D., Mothé-Diniz, T., Angeli, C. A., & Betzler, A. S. 1999, *A&AS*, 134, 463
- Groussin, O., A'Hearn, M. F., Li, J.-Y., Thomas, P. C., Sunshine, J. M., Lisse, C. M., Meech, K. J., Farnham, T. L., Feaga, L. M., & Delamere, W. A. 2007, *Icarus*, 187, 16
- Harris, A. W. 1998, *Icarus*, 131, 291
- Hsieh, H. H., & Jewitt, D. 2006, *Asteroids, Comets, Meteors*, 229, 425
- Hsieh, H. H., & Jewitt, D. 2006, *Science*, 312, 561
- Hsieh, H. H., Jewitt, D. C., & Fernández, Y. R. 2004, *AJ*, 127, 2997
- Jewitt, D. C. 2002, *AJ*, 123, 1039
- Jewitt, D., & Hsieh, H. 2006, *AJ*, 132, 1624
- Kasuga, T., & Jewitt, D. 2008, *AJ*, 136, 881
- Kinoshita, D., Ohtsuka, K., Sekiguchi, T., Watanabe, J., Ito, T., Arakida, H., Kasuga, T., Miyasaka, S., Nakamura, R., & Lin, H.-C. 2007, *A&A*, 466, 1153
- Lamy, P. L., Toth, I., Fernández, Y. R., & Weaver, H. A. 2004, *Comets II*, 223
- Landolt, A. U. 1992, *AJ*, 104, 340
- Lazzaro, D., Angeli, C. A., Carvano, J. M., Mothé-Diniz, T., Duffard, R., & Florczak, M. 2004, *Icarus*, 172, 179

- Levison, H. F., Bottke, W. F., Nesvorný, D., Morbidelli, A., & Gounelle, M. 2008, LPI Contributions, 1405, 8156
- Licandro, J., Pinilla-Alonso, N., de León, J., Campins, H., Boehnhardt, H., Tozzi, G., Hainaut, O., & Mothé-Diniz, T. 2007a, Bulletin of the American Astronomical Society, 38, 470
- Licandro, J., Campins, H., Mothé-Diniz, T., Pinilla-Alonso, N., & de León, J. 2007b, A&A, 461, 751
- Morrison, D. 1977, ApJ, 214, 667
- Oke, J. B., Cohen, J. G., Carr, M., Cromer, J., Dingizian, A., Harris, F. H., Labrecque, S., Lucinio, R., Schaal, W., Epps, H., & Miller, J. 1995, PASP, 107, 375
- Reach, W. T., Kelley, M. S., & Sykes, M. V. 2007, Icarus, 191, 298
- Rieke, G. H., et al. 2004, ApJS, 154, 25
- Tedesco, E. F., Noah, P. V., Noah, M., & Price, S. D. 2004, NASA Planetary Data System, IRAS-A-FPA-3-RDR-IMPS-V6.0, 12
- Tholen, D. J., Barucci, M. A. 1989, Asteroids II, 1139
- Tonry, J. L., Burke, B. E., Luppino, G., & Kaiser, N. 2004, Scientific Detectors for Astronomy, The Beginning of a New Era, 300, 385
- Werner, M. W., et al. 2004, ApJS, 154, 1

Table 1. Spitzer Observations

Object	Date	UT	R^a	Δ_{Sp}^b	α_{Sp}^c	m_R^d
133P/Elst-Pizarro	2005 Apr 11	08:01:11	3.596	3.046	14.6	21.56 ± 0.15
	2005 Apr 11	08:04:49	3.596	3.046	14.6	21.63 ± 0.15
	2005 Apr 11	08:08:30	3.596	3.046	14.6	21.70 ± 0.15
176P/LINEAR	2007 Jan 01	00:49:12	3.162	2.541	16.2	20.58 ± 0.11
	2007 Jan 01	05:22:13	3.163	2.539	16.1	20.21 ± 0.11

^aHeliocentric distance in AU

^bDistance from Spitzer in AU

^cSolar phase angle (Sun-object-Spitzer) in degrees

^dExpected R -band magnitude as calculated from rotational-phase information inferred from the infrared data and observationally-determined H, G phase functions (Fig. 2). Listed errors account for uncertainties in both rotational phase and phase function solutions.

Table 2. Albedos and Radii Computed from Optical and Infrared Observations

Object	$\eta = 0.8^a$			$\eta = 1.0^a$			$\eta = 1.2^a$		
	$F_{24\mu m}$	r_e	p_R	$F_{24\mu m}$	r_e	p_R	$F_{24\mu m}$	r_e	p_R
133P/Elst-Pizarro	6.4 ± 0.1	1.78	0.054	6.5 ± 0.1	1.94	0.045	6.5 ± 0.1	2.09	0.039
	6.0 ± 0.1	1.72	0.054	6.0 ± 0.1	1.88	0.045	6.1 ± 0.1	2.03	0.039
	5.7 ± 0.1	1.67	0.054	5.7 ± 0.1	1.83	0.045	5.7 ± 0.1	1.97	0.039
176P/LINEAR	10.4 ± 0.2	1.72	0.068	10.5 ± 0.2	1.87	0.058	10.5 ± 0.2	2.01	0.050
	14.6 ± 0.2	2.04	0.068	14.7 ± 0.2	2.22	0.058	14.7 ± 0.2	2.38	0.050

^aAssumed η value used to compute aperture- and color-corrected 24 μm flux ($F_{24\mu m}$) in mJy (where uncertainties are estimated from sky background statistics), effective radius (r_e) in km, and geometric R -band albedo (p_R)

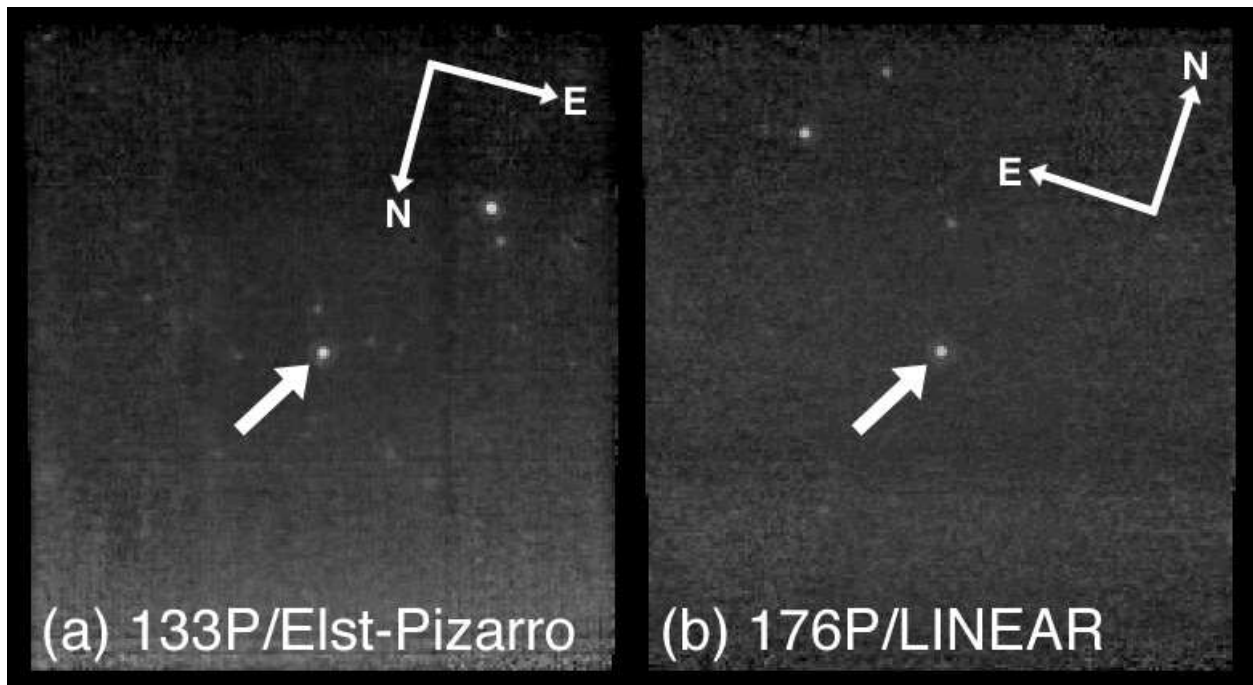


Fig. 1.— Composite (PBCD) $24\ \mu\text{m}$ images of (a) 133P/Elst-Pizarro (166 s total exposure time) and (b) 176P/LINEAR (48 s total exposure time), indicated by arrows, obtained using MIPS on Spitzer. Both objects are point sources with no indication of cometary activity. Each panel is ~ 7.5 by 8.2 in size.

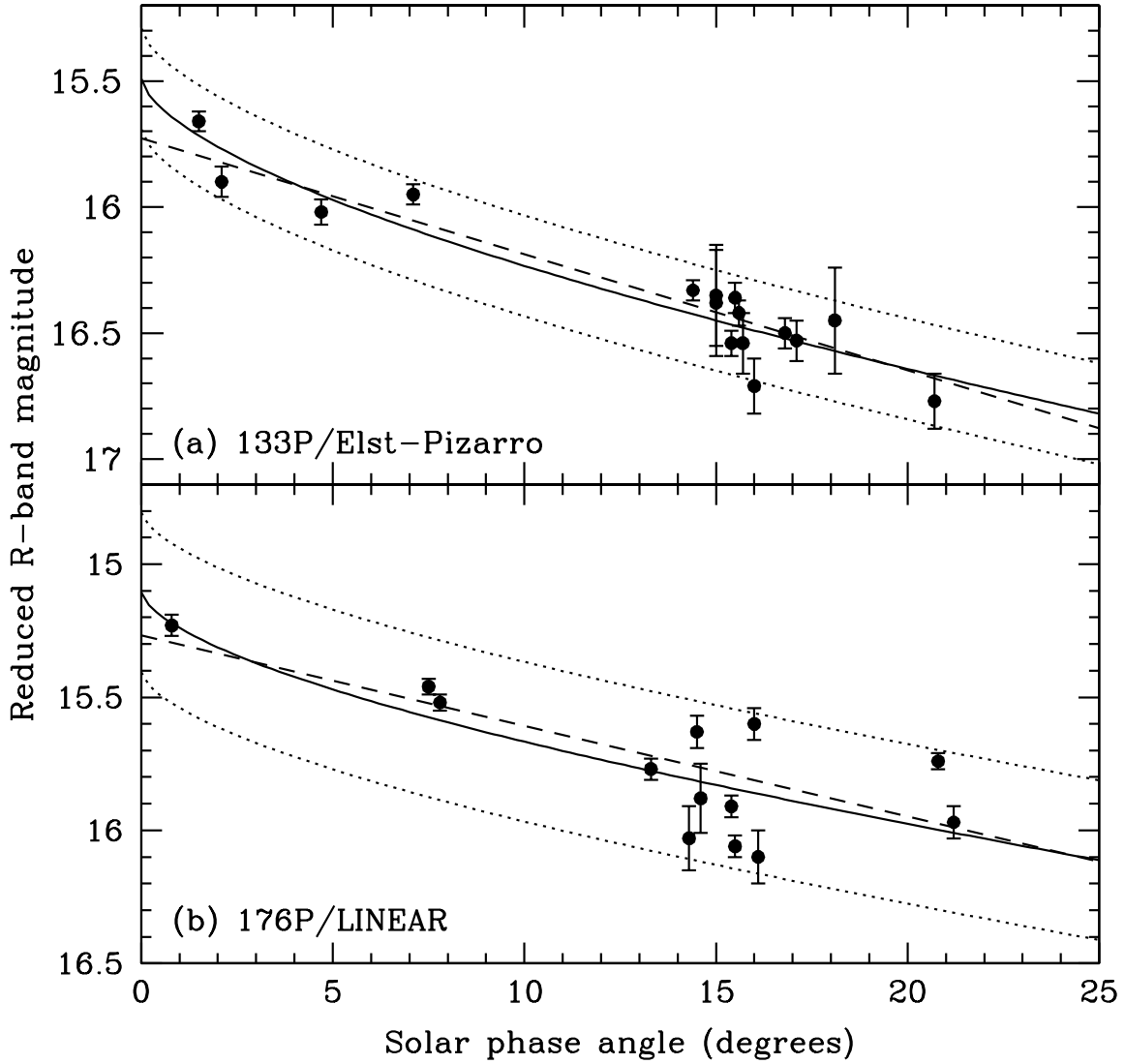


Fig. 2.— Phase function solutions for (a) 133P/Elst-Pizarro and (b) 176P/LINEAR, with best-fit IAU phase laws plotted as solid lines and best-fit linear phase functions plotted as dashed lines. Dotted lines indicate the expected range of brightness deviations from the IAU phase law due to rotation of the body. Observed reduced R -band magnitudes are plotted as solid circles.

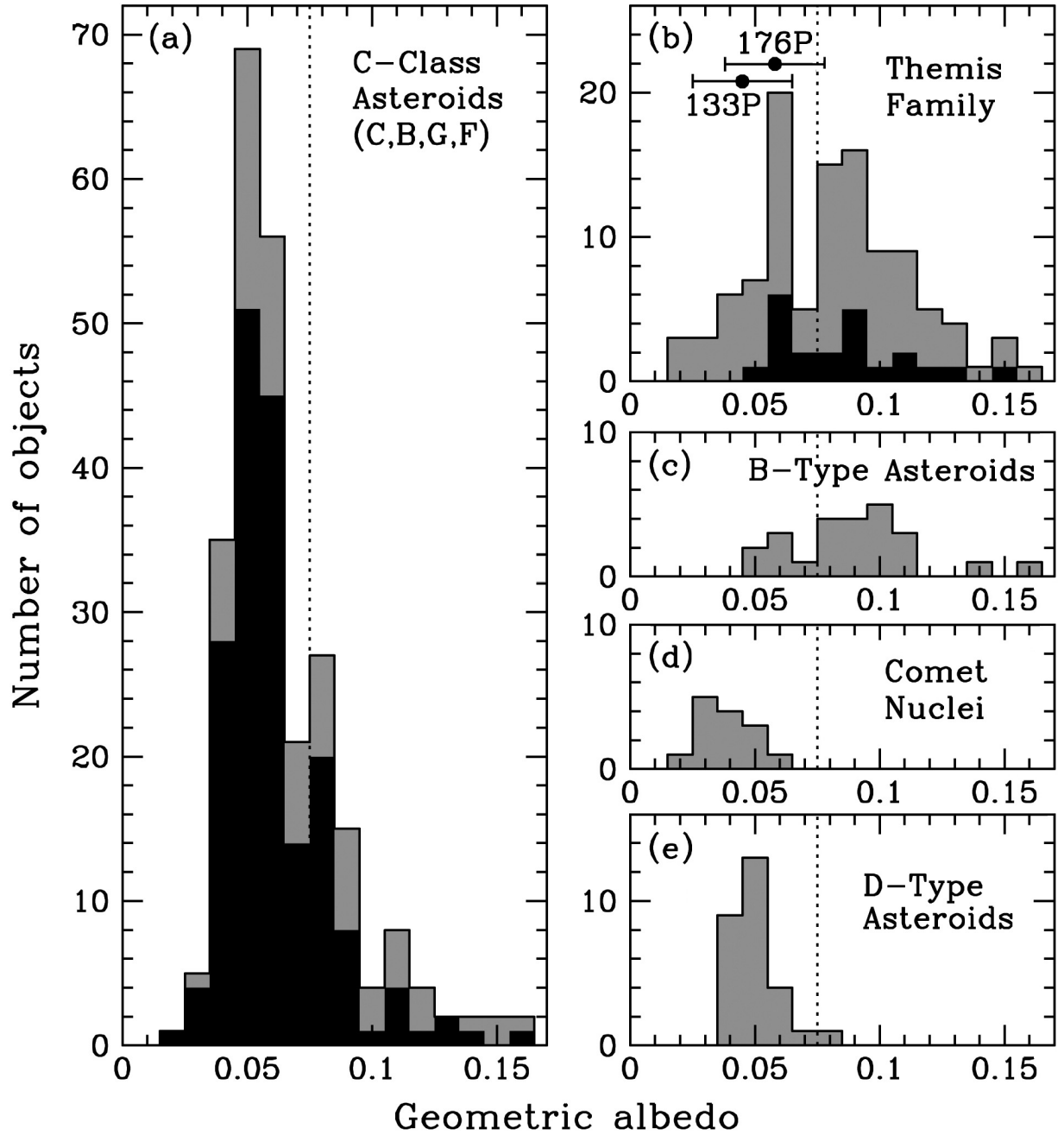


Fig. 3.— Histograms showing albedo distributions for (a) C-class (C-, B-, G-, or F-type) asteroids, where the superimposed black-shaded histogram only includes objects explicitly classified as C-type asteroids, (b) dynamical members of the Themis asteroid family, where the superimposed black-shaded histogram only includes those Themis members with measured albedos that have been classified as C-class asteroids (not all have been assigned taxonomic classes to date, however), (c) B-type asteroids, (d) active comet nuclei, and (e) D-type asteroids. All taxonomic classifications follow the Tholen system (Tholen & Barucci 1989; Lazzaro *et al.* 2004). Comet nucleus albedos are from Lamy *et al.* (2004) and Brownlee *et al.* (2004), while all other albedo values are from the IRAS Minor Planet Survey (Tedesco *et al.* 2004). Objects with $p < 0.075$, designated as “cometary” by Fernández *et al.* (2005), are to the left of the dotted lines.